International Journal of Automotive Technology, Vol. 10, No. 3, pp. 329–339 (2009)
DOI 10.1007/s12239–009–0038–9

1229–9138/2009/046–08

IMPACT BEHAVIOR MODELING OF MOTORCYCLE FRONT WHEEL-TIRE ASSEMBLY

K. S. TAN[1,2], S. V. WONG[1,3)*], R. S. RADIN UMAR[3)], A. M. S. HAMOUDA[1)] and N. K. GUPTA[4)]

[1)]Department of Mechanical and Manufacturing Engineering, Faculty of Engineering, Universiti Putra Malaysia, UPM Serdang, 43400 Selangor, Malaysia
[2)]Department of Mechanical Engineering, Faculty of Engineering, National Defence University of Malaysia, Sungai Besi Camp, 57000 Kuala Lumpur, Malaysia
[3)]Malaysian Institute of Road Safety Research, 43000 Kajang, Selangor, Malaysia
[4)]Department of Applied Mechanics, Indian Institute of Technology, Hauz Khas, New Delhi 110016, India

(Received 18 May 2007; Revised 7 August 2008)

ABSTRACT–Experiments were conducted to investigate the influence of certain parameters that affect the impact response of the motorcycle front wheel-tire assembly under various impact conditions. Impact tests were conducted according to 2_V^{5-1} fractional factorial design using a pendulum impact test apparatus with impact speed, impact mass, tire inflation pressure level, striker geometry, and impact location as design factors. Significant factors influencing the response of the wheel-tire assembly were identified. Coefficients for each factor were also determined, and empirical models were then developed for each response. An analysis indicates that the developed models fit well within the experimental ranges of the respective factors. However, for several interaction effects, the models become unrealistic, whereby they give certain deformation values when approaching zero impact mass and/or zero impact velocity. This is not consistent with the mechanics of the physical world, as there should not be any significant deformation when delivered impact energy is small enough. Efforts have been made in developing better models to resolve the inconsistency and to include a wider range, especially considering the case of the lower limit of experimental factors, which are an impact mass of 51.18 kg and/or an impact velocity of 3 m s^{-1} (10.8 km/h) down to zero. The minimum amount of impact energy required to produce the onset of observable deformation on the wheel was incorporated in the development of new models. Finally, the present models have been developed not only to cover the lower regions but also to range up to the upper limits of the factors, which are an impact mass of 101.33 kg and an impact velocity of 6 m s^{-1} (21.6 km/h).

KEY WORDS : Impact behavior, Wheel-tire assembly, Modeling, Motorcycle, DOE

1. INTRODUCTION

Previous work has revealed that frontal components of a motorcycle possess a high rate of exposure to damage (Harms, 1989; Otte *et al*., 1981; Sporner *et al*., 1995; Whitaker, 1980) and that frontal collision of motorcycles into passenger cars constituted a major percentage of total traffic accidents (Hight *et al*., 1986; Pang *et al*., 1999; Whitaker, 1980). As a motorcycle front wheel-tire assembly usually makes the first and most direct contact with the opponent vehicle in a frontal collision, studies of the interaction mechanism and impact response this assembly such collisions are thus worth performing. This would provide useful information in the effort to improve the safety features of vehicles and to understand motorcycle and rider dynamics at impact conditions.

It was found that the dynamics of the motorcycle and the dummy depend initially on the collapsing characteristics of the front wheel (Yettram *et al*., 1994). It has also been demonstrated that it is important to determine the reaction force of the front tire in the simulation of motorcycle to car crash, as the force influences the subsequent motions of the motorcycle and the rider (Fujii, 2003). In other research of the motorcycle front wheel-tire assembly (Tan *et al*., 2006), a strong correlation has been found between the absorbed impact energy and the impact response in terms of maximum residual crush and deformed area of the wheel, through a regression study using an experimental approach with various impact conditions.

Obviously, a crash of a motorcycle into a car or any barrier is a complex event involving various parameters that would influence the response of the wheel-tire assembly to certain extent. It would be more beneficial to reduce the scope and focus on some predominant parameters in order to effectively study their effects. The factorial experiment method has been utilized for this purpose in the present study. In this paper, the corresponding experimental works will first be described, followed by the presentation

**Corresponding author:* e-mail: wongsv@miros.gov.my

of initial empirical models resulting from factorial analysis. The inconsistency of the initial models to the real physical conditions was identified for some interaction effects, and these will be illustrated in graphs and discussed. The paper will then be devoted to the process of developing the enhanced models that satisfy the physical conditions and cover the full spectrum of the experimental range. Finally, the resulting enhanced models will be presented and discussed.

2. EXPERIMENTAL PROCEDURES

Five factors were considered in the present study: impact speed, impact mass, inflation pressure level of the tube, contact geometry of the striker, and offset distance of the impact from axle level. A design of experiments (DOE) method has been used instead of a classic one-at-a-time parameter approach. The software Minitab (Minitab, 2000) was used for the entire process of experimental design and analysis. The impact tests were performed based on 2_V^{5-1} fractional factorial design (Montgomery, 2001), with the corresponding values of factor levels presented in Table 1.

In order to better match the impact test requirements for the present study, an impact test apparatus, MechT™ Impactor, model PutrArm 275 (Tan *et al.*, 2004), as shown in Figure 1(a), was specifically designed and developed. The arrangement of the wheel-tire assembly on the wheel holding device is depicted in Figure 1(b). Only the spoked wheel design is considered in the present study, as it represents the most commonly used type of wheel design on most motorcycles. The specific model of test specimen selected is the original front wheel-tire assembly of Malaysian motorcycle, KRISS 110.

The specification of the rim is Union Cycle, rim size 1.40×17 inches, while the tire model is Dunlop TT100 70/90. The wheel was installed with all components, including rim, spokes, hub, bearings, oil seal, and spacer, but excluding brake shoes. The wheels were laced to an identical pattern and trued with extra care, as a different cross-pattern of the spokes or improper truing may result in a different strength of the wheel.

The combination of design factors in each test run is indicated in Table 2, under the column of "Factor Level". Conventionally, the plus (+) and minus (−) signs are used to indicate high and low levels of each design factor, respectively. Based on the DOE principle (Montgomery, 2001), with 2_V^{5-1} fractional factorial design, the level of one of the factors, which is D in the present study, has to be derived from others by multiplying the plus (+) and/or minus (−) signs with typical mathematical manipulation. For example, from Table 2, treatment combination number 5, the test is to be run with S at low, M at low, P at high and G at low level. By multiplying the signs, (−)*(−)*(+)*(−), gives a minus (−) sign, or low level of D.

Table 1. Design factors and the corresponding values for low and high levels.

Factor	Notation	Low (−)	High (+)
Impact speed (ms^{-1})	S	3	6
Impact mass (kg)	M	51.18	101.33
Tyre pressure (kPa)	P	148	252
Striker contact geometry (m)	G	radius=0.03	radius=0.10
Impact offset distance (m)	D	height=0	height=0.108

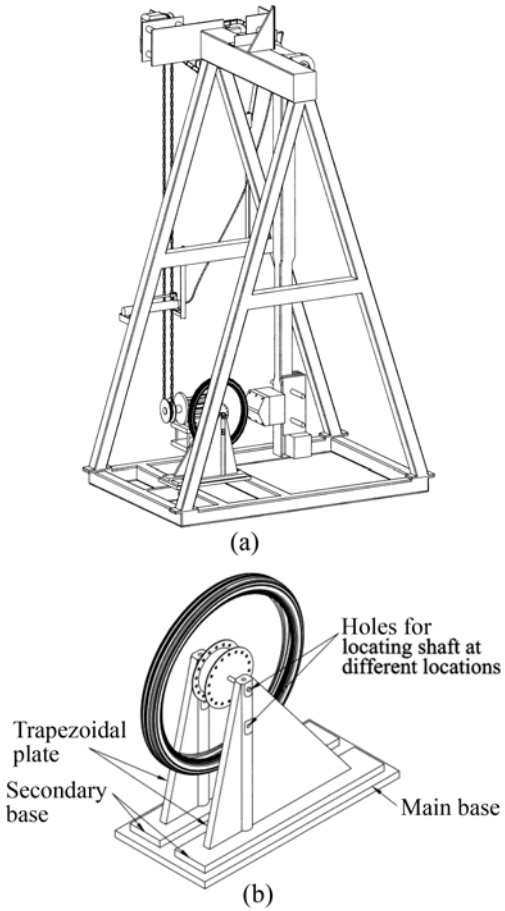

Figure 1. (a) Experimental setup of impact test on a motorcycle front wheel-tire assembly; (b) arrangement of wheel-tire assembly on the wheel holding device.

Upon completing each impact test run, measurements were taken according to the selected response variables, namely, maximum residual crush (δ) and normalized area of deformation ($\Delta\bar{A}$). The maximum residual crush (δ) is defined as the final residual radial displacement of the rim's outermost deformed edge from its original shape after impact, as depicted in Figure 2. The definition for $\Delta\bar{A}$ is expressed by Equation (1) as

$$\Delta\bar{A}=\frac{\Delta A}{A} \tag{1}$$

Table 2. Experimental data for the response δ.

Design	Treatment combination	Factor level					Maximum crush, δ (mm)			
		S	*M*	*P*	*G*	*D=SMPG*	Replicate 1	Replicate 2	Replicate 3	Replicate 4
1	*d*	−	−	−	−	+	4 (2)	5 (28)	4 (37)	4 (55)
2	*s*	+	−	−	−	−	81 (3)	86 (18)	82 (21)	83 (27)
3	*m*	−	+	−	−	−	35 (1)	37 (10)	40 (56)	40 (57)
4	*smd*	+	+	−	−	+	125 (4)	137 (25)	121 (43)	131 (50)
5	*p*	−	−	+	−	−	3 (7)	4 (8)	3 (14)	4 (52)
6	*spd*	+	−	+	−	+	82 (6)	74 (49)	67 (53)	69 (54)
7	*mpd*	−	+	+	−	+	19 (15)	19 (17)	22 (34)	16 (61)
8	*smp*	+	+	+	−	−	148 (5)	141 (23)	148 (40)	148 (62)
9	*g*	−	−	−	+	−	4 (13)	4 (16)	5 (20)	5 (26)
10	*sgd*	+	−	−	+	+	93 (24)	80 (29)	88 (39)	85 (63)
11	*mgd*	−	+	−	+	+	28 (12)	28 (35)	28 (41)	31 (47)
12	*smg*	+	+	−	+	−	145 (9)	148 (46)	146 (59)	139 (60)
13	*pgd*	−	−	+	+	+	4 (11)	3 (22)	3 (42)	3 (64)
14	*spg*	+	−	+	+	−	67 (30)	69 (36)	61 (38)	80 (44)
15	*mpg*	−	+	+	+	−	24 (19)	29 (31)	27 (33)	32 (51)
16	*smpgd*	+	+	+	+	+	146 (32)	142 (45)	140 (48)	145 (58)

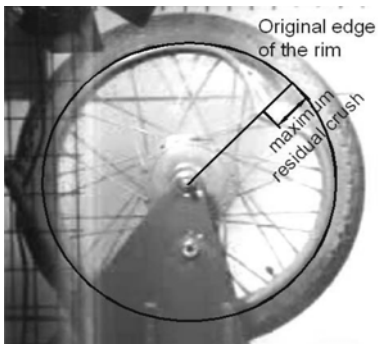

Figure 2. Definition of residual maximum crush, δ: final residual radial displacement of the rim's outermost deformed edge from its original shape.

where the A and ΔA are defined as illustrated in Figure 3. Experimental data, i.e., the measurements of δ and ΔA, are summarized in Tables 2 and 3, respectively. The number in the bracket next to the experimental data in each table refers to the actual run order of the impact test in DOE. As there are 4 replicates for each test configuration, which were conducted randomly, such labeling of the test run order is helpful for tracing back a particular wheel.

3. INITIAL EMPIRICAL MODELS

Based on the factorial analysis, significant factors that affect the impact response of the wheel-tire assembly were identified. The results of the analysis in terms of the coefficients of factors that are statistically significant at 95% confidence level and the corresponding P-values are summarized in

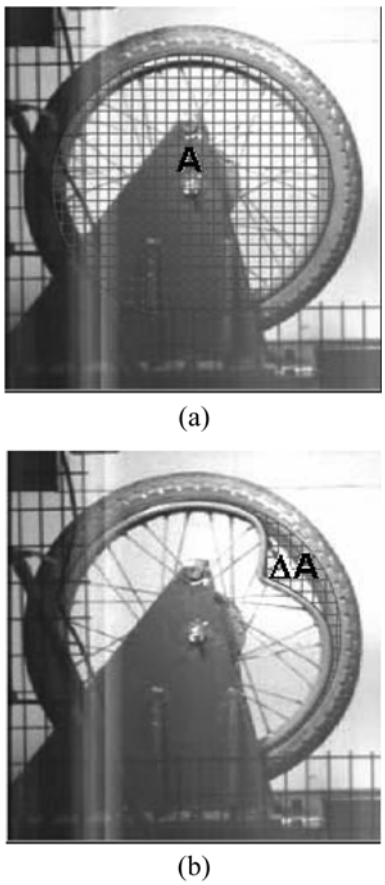

Figure 3. Definitions for (a) A: total projected area of original wheel enclosed by the outer edge of the rim; (b) ΔA: projected area of deformation.

Table 3. Experimental data for the response $\Delta\tilde{A}$.

Design	Treatment combination	Factor level					Normalized area of deformation, $\Delta\tilde{A}$			
		S	*M*	*P*	*G*	*D=SMPG*	Replicate 1	Replicate 2	Replicate 3	Replicate 4
1	*d*	−	−	−	−	+	0.0061(2)	0.0063 (28)	0.0063 (37)	0.0062 (55)
2	*s*	+	−	−	−	−	0.0616 (3)	0.0659 (18)	0.0643 (21)	0.0682 (27)
3	*m*	−	+	−	−	−	0.0230 (1)	0.0247 (10)	0.0278 (56)	0.0263 (57)
4	*smd*	+	+	−	−	+	0.3008 (4)	0.1921 (25)	0.2874 (43)	0.3224 (50)
5	*p*	−	−	+	−	−	0.0037 (7)	0.0033 (8)	0.0037 (14)	0.0034 (52)
6	*spd*	+	−	+	−	+	0.0668 (6)	0.0622 (49)	0.0430 (53)	0.0432 (54)
7	*mpd*	−	+	+	−	+	0.0172 (15)	0.0183 (17)	0.0156 (34)	0.0235 (61)
8	*smp*	+	+	+	−	−	0.1586 (5)	0.1507 (23)	0.1510 (40)	0.1550 (62)
9	*g*	−	−	−	+	−	0.0057 (13)	0.0048 (16)	0.0058 (20)	0.0040 (26)
10	*sgd*	+	−	−	+	+	0.0719 (24)	0.0651 (29)	0.0745 (39)	0.0658 (63)
11	*mgd*	−	+	−	+	+	0.0212 (12)	0.0205 (35)	0.0222 (41)	0.0220 (47)
12	*smg*	+	+	−	+	−	0.1641 (9)	0.1561 (46)	0.1665 (59)	0.1933 (60)
13	*pgd*	−	−	+	+	+	0.0066 (11)	0.0054 (22)	0.0050 (42)	0.0068 (64)
14	*spg*	+	−	+	+	−	0.0527 (30)	0.0529 (36)	0.0808 (38)	0.0673 (44)
15	*mpg*	−	+	+	+	−	0.0179 (19)	0.0197 (31)	0.0337 (33)	0.0244 (51)
16	*smpgd*	+	+	+	+	+	0.1662 (32)	0.3094 (45)	0.3416 (48)	0.1650 (58)

Table 4. Coefficients and P-values of significant factors for the response variable $\sqrt{\delta}$ resulted from factorial analysis.

Factor	*S*	*M*	*P*	*SM*	*SP*	*SD*	*MD*	*GD*
Coefficient	0.066	0.00253	−0.0003	−0.000061	0.000039	0.0286	−0.00456	2.15
P-value	0.000	0.000	0.000	0.047	0.009	0.009	0.000	0.000

Table 5. Coefficients and P-values of significantfactors for the response variable resulted from factorial analysis.

Factor	*S*	*M*	*P*	*G*	*D*	*SM*	*MG*	*MD*	*PG*
Coefficient	0.964	0.041	−0.00496	−5.85	3.53	−0.00262	−0.0422	−0.0365	0.0482
P-value	0.000	0.000	0.000	0.007	0.000	0.000	0.018	0.003	0.000

Tables 4 and 5 for the response variables $\sqrt{\delta}$ and $\ln \Delta\tilde{A}$, respectively. Empirical models were also developed for predicting the post-impact deformation on a motorcycle spoked wheel-tire assembly under various impact testing conditions. The models were established by multiplying each factor with the respective coefficient and summing all the terms. The choices of hierarchical and non-hierarchical models (Montgomery, 2001) were also taken into consideration before being finalized.

The final empirical models for predicting the impact response of the wheel-tire assembly in terms of maximum residual crush and normalized deformed area are given by Equations (2) and (3), respectively.

$$\begin{aligned}\sqrt{\delta} = &-0.219 + 0.0660*S + 0.00253*M \\ &- 0.0003*P - 0.000061*S*M \\ &+ 0.000039*S*P + 0.0286*S*D \\ &- 0.00456*M*D + 2.15*G*D\end{aligned} \tag{2}$$

$$\begin{aligned}\ln\Delta\tilde{A} = &-9.09 + 0.964*S + 0.0410*M \\ &- 0.00496*P - 5.85*G + 3.53*D \\ &- 0.00262*S*M - 0.0422*M*G \\ &- 0.0365*M*D + 0.0482*P*G\end{aligned} \tag{3}$$

For obvious reasons, the developed empirical model for the response δ (Equation 2) is limited only for $\sqrt{\delta} \geq 0$. For Equation (3), considering that the deformed area (Ä*A*) can never exceed the original undeformed area (*A*), the value of the response $\Delta\tilde{A}$ is always less than or equal to 1. Thus, the developed empirical model (Equation 3) is valid only if $\ln \Delta\tilde{A} \leq 0$.

To better visualize the impact response of the wheel-tire assembly, several curves have been generated from the corresponding models for the significant interaction effects. A graph for impact speed-impact mass (*SM*) interaction effect based on Equation (2) is shown in Figure 4, where the maximum residual crush of the rim varies with *S* for several values of *M*, with other factors constant at set

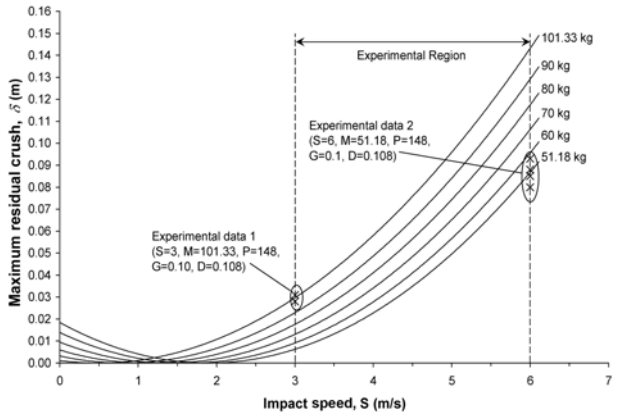

Figure 4. Plot of δ versus S at P=148 kPa, G=0.10 m, and D=0.108 m for M 51.18, 60, 70, 80, 90, and 101.33 kg.

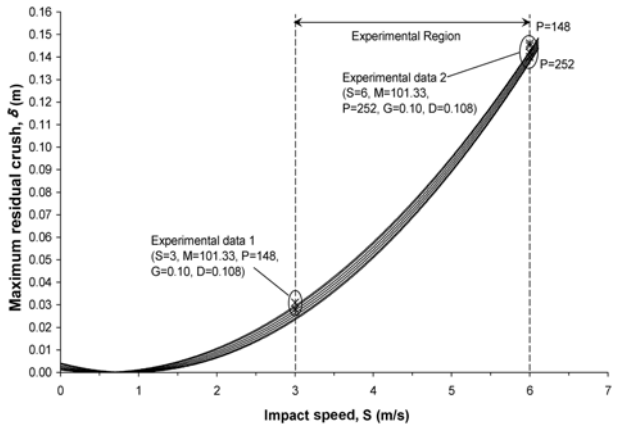

Figure 5. Plot of δ versus S at M=101.33 kg, G=0.10 m, and D=0.108 m for P=148, 160, 180, 200, 220, 240, and 252 kPa.

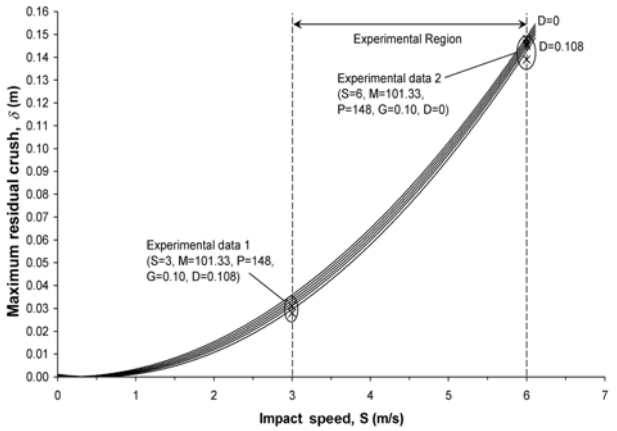

Figure 6. Plot of δ versus S at M=101.33 kg, G=0.10 m, and P=148 kPa for D=0, 0.02, 0.04, 0.06, 0.08, and 0.108 m.

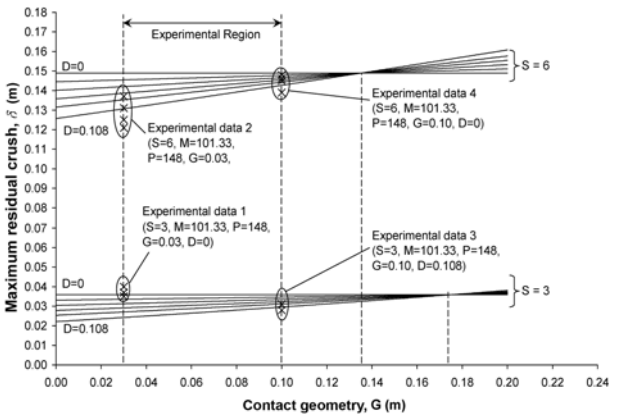

Figure 7. Plot of δ versus G at M=101.33 kg, P=148 kPa, and S=3 and 6 m s^{-1} for D=0, 0.02, 0.04, 0.06, 0.08, and 0.108 m.

values. Graphs for other interaction effects for maximum residual crush and for normalized area of deformation were also plotted accordingly and are presented in Figures 5 to 8 based on Equation (2) and Figures 10 to 13 based on Equation (3), respectively. To compare the responses predicted by the equations, the related data at certain experimental levels were represented on each graph by cross marks.

It can be observed from Figure 4 that the curves intersect the S-axis at a lower value as impact mass increases. This is consistent with the common physical condition that with higher impact mass, lower impact speed is required to produce the impact energy needed to cause the same degree of residual crush on the rim.

In Figure 5, it is noticeable from various intersection points of the plotted curves on the S-axis that the higher the tire inflation pressure level, the higher the threshold value of impact speed required to cause an initial observable post-impact residual crush on the rim. This is simply because at higher inflation levels, the tire provides a greater stiffness and better cushioning to reduce the degree of wheel deformation under identical impact loads.

Figure 6 shows that intersections on abscissa occur at higher values of S as the D value increases. The reason for this observation is that in an offset impact situation, as a result of reduced effective force, a higher impact velocity is thus required to produce an identical initial observable crush on the rim compared to the impact that is directed radially towards an axle, provided that other parameters remain constant.

When interacting with G, the influence of D was reduced from low to high G level, as illustrated in Figure 7, where the gap between the curves decreased as G increased. This is due to the progressive shifting of contact geometry from the inclined flat triangular striker to the rounded surface semi-cylindrical striker, which is more effective in causing an indentation or bending on the rim in offset impact. Conversely, when interacting with M, the D factor demonstrated the opposite effect at low vs. high M level, as depicted in Figure 8.

The residual crush decreases with the offset impact distance at high M level, and vice versa at low M level. The

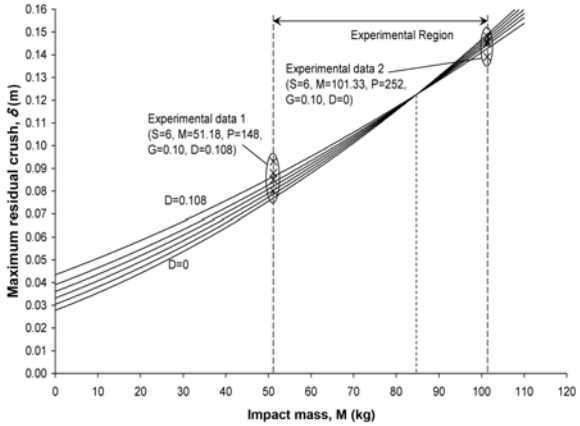

Figure 8. Plot of δ versus M at S=6 m s^{-1}, P=148 kPa, and G=0.10 m for D=0, 0.02, 0.04, 0.06, 0.08, and 0.108 m.

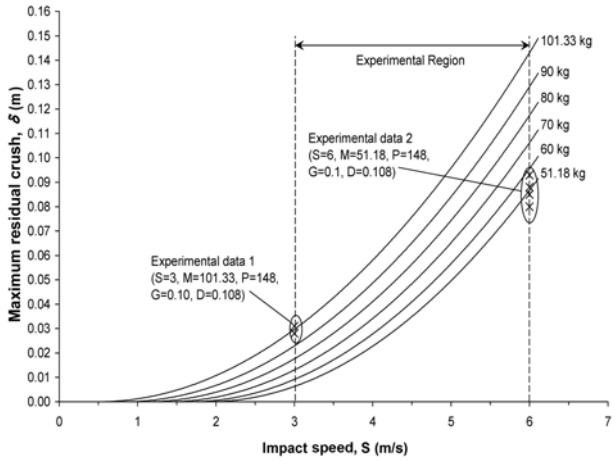

Figure 9. Plot of δ versus S at P=148 kPa, G=0.10 m, and D=0.108 m for M=51.18, 60, 70, 80, 90, and 101.33 kg (for $\sqrt{\delta} \geq 0$).

transition value of impact mass where the D effect inverted is approximately 84 kg. However, further experimental work and investigation is needed in order to explain the implication of this transition point.

The post-impact residual crush is always towards the center of the rim, or in the same direction with the impact. It is not realistic for the rim to spring back and crush in the direction opposite to the impact. Thus, the lower range of the response curves corresponding to $\sqrt{\delta} < 0$ should be removed, as shown in Figure 9 as ϕ_T example of the SM interaction.

From Figure 8, it is apparent that when the curves are extrapolated towards zero impact mass, they do not reach zero residual crush but intersect with the δ-axis at the value of about 0.030 to 0.045 m for the values of D ranging from 0 to 0.108 m, respectively. This is not physically realistic, as there should be insignificant or no deformation when impact mass is small enough ($M \neq 0$). Indeed, the curves should intersect the positive M-axis, giving the minimum impact mass required to cause the initial significant residual

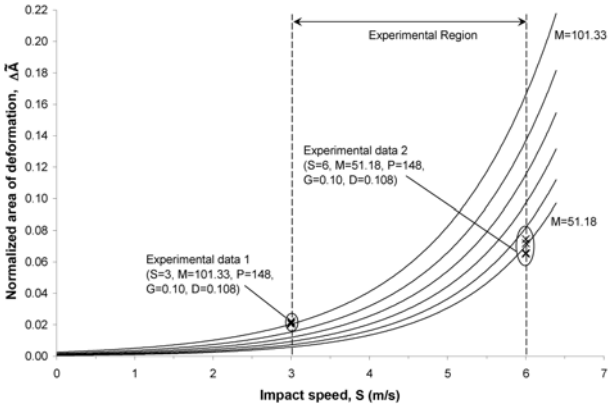

Figure 10. Plot of $\Delta\tilde{A}$ versus S at P=148 kPa, G=0.10 m, and D=0.108 m for M=51.13, 60, 70, 80, 90, and 101.33 kg.

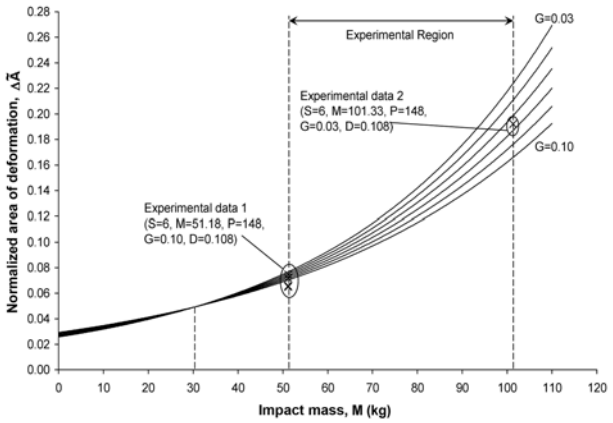

Figure 11. Plot of $\Delta\tilde{A}$ versus M at S=6 m s^{-1}, P=148 kPa, and D=0.108 m for G=0, 0.02, 0.04, 0.06, 0.08, and 0.10 m.

crush on the rim for a given impact speed.

The response of $\Delta\tilde{A}$ to the interaction of SM is depicted in Figure 10. A typical curve distribution can be observed from the graph, whereby an increase in the area of deformation is always accompanied by an increase of the impact mass and impact speed. For an impact mass within the experimental range, increasing the contact surface of the striker is expected to reduce the area of deformation sustained by the wheel.

The effect of G is highly influenced by the impact mass. As presented in Figure 11, the effect of G decreases significantly as impact mass is reduced to a low level and becomes relatively insignificant when impact mass falls below about 40 kg. Although there is a transition point at about 31 kg, where the G factor has the opposite effect on the response, the implication might not be important because the effect is not significant. When effect D interacts with effect M, as presented in Figure 12, the interaction is relatively insignificant at a high M level. For impact mass of about 90 kg and below, increasing the offset distance of impact location reduces the effectiveness of the striker in deforming the rim, resulting in lower $\Delta\tilde{A}$ value. A transition of impact mass in the MD interaction occurs at about

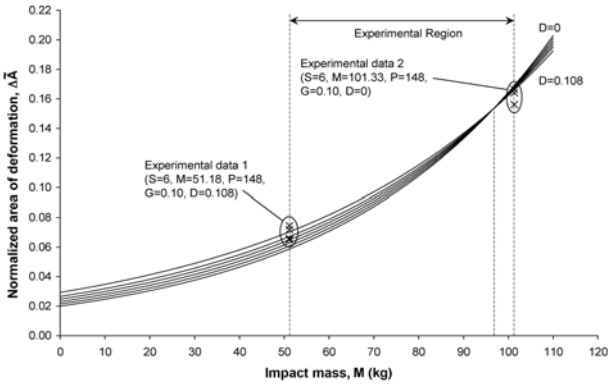

Figure 12. Plot of $\Delta\tilde{A}$ versus M at S=6 m s^{-1}, P=148 kPa, and G=0.10 m for D=0, 0.02, 0.04, 0.06, 0.08, and 0.108 m.

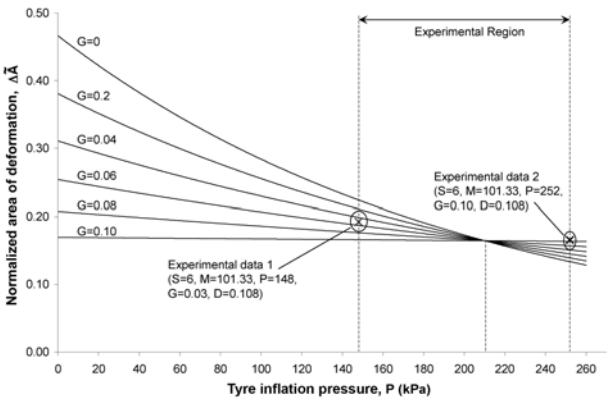

Figure 13. Plot of $\Delta\tilde{A}$ versus P at S=6 m s^{-1}, M=101.33 kg, and D=0.108 m for G=0, 0.02, 0.04, 0.06, 0.08, and 0.10 m.

97 kg.

A transition in tire pressure level also occurs in the PG interaction at approximately 210 kPa (Figure 13). This is very close to the manufacturer's recommended tire pressure level, 200 kPa. However, the insights of implication of all transition phenomena require further investigations to be carried out.

It can be seen that the inconsistency with real physical conditions, as in the case for δ, also occurred for $\Delta\tilde{A}$. For the SM interaction (Figure 10), as the curves are extrapolated across the relation towards the $\Delta\tilde{A}$-axis, they intersect the axis very close to zero. However, it is more appropriate to intersect the positive S-axis and indicate a specific value of S_{cr}. For the MG interaction (Figure 11) and MD interaction (Figure 12), the curves also do not intersect at zero or positive M-axis near zero but at values of around 0.03 units for D and G values of 0 to 0.108 m and 0 to 0.10 m, respectively, indicating a deviation from the common understanding of mechanics.

4. DEVELOPMENT OF ENHANCED MODELS

It is important to emphasize that with two-level factorial design, each factor has only two levels and is assumed to vary linearly within the experimental region. The two-level factorial design is unable to explore fully a wide range in the factor space. The models resulted from factorial analysis are also valid within the experimental range only, with linear relationship as the assumption. Regression analyses for the initial models produced good results within experimental range, with R^2 of 99.94% and 99.59%, respectively. However, the models were found to not satisfy basic physical conditions for some interaction effects, as discussed in Section 3. Additional efforts have thus been exerted to resolve the problems and attempted to include a wider range, considering especially the cases within the lower limits of experimental factors, which are impact mass of 51.18 kg and impact velocity of 3 m s^{-1} (10.8 km/h), down to their respective zero values. New models have been finally developed to include not only the lower regions but also the ranges up to the upper limits of the factors, which are impact mass of 101.33 kg and impact velocity of 6 m s^{-1} (21.6 km/h). The following sections are devoted to the discussion on the process of developing the enhanced models that satisfy the physical condition and cover the whole spectrum of the experimental range.

4.1. Considerations and Method of Approach

The amount of impact energy delivered by the impact test apparatus plays the key role in determining the deformation sustained by the wheel-tire assembly during impact. The threshold value of the impact energy to produce the onset of observable deformation on the wheel has been incorporated in the development of enhanced models. For a subject to undergo any deformation when subjected to loading, there is always a minimum amount of energy required, which corresponds to elastic deformation before the subject starts to deform plastically. No permanent deformation will be observed, and thus no energy dissipated, if the delivered loading energy is below that critical amount. Similarly, to produce the initial observable deformation on the wheel, a certain amount of minimum impact energy is essential to account for the elastic phase. This amount of energy is referred to here as the threshold value of the impact energy and is termed critical impact energy (E_{cr}).

The critical impact energy has a very important implication in that it is related to a certain threshold value of impact mass, M_{cr}, and impact velocity, S_{cr}, as expressed in the kinetic energy relation in Equation (4):

$$E_{cr}=\frac{1}{2}M_{cr}S_{cr}^2 \tag{4}$$

Thus, it is reasonable for E_{cr} to be incorporated into the model development. If E_{cr} is equal to the impact energy provided, E, or as a mathematical expression, $E_{cr}=E=\frac{1}{2}MS^2$, and since E_{cr} is a constant, then there will be one M_{cr} value for a specific S value, and one S_{cr} value for a specific M value. Thus, if E is subtracted from E_{cr} (or inversely, E_{cr} subtracted from E), this may lead to the intersection of the curve at the M-axis and S-axis on the relevant graphs. The

relation $E–E_{cr}$ was selected arbitrarily. By careful consideration, it will revealed that any term or equation, when multiplied by the relation ($E–E_{cr}$), as its zero solution will give a certain value of M_{cr} (for $E–½M_{cr}S^2$) and S_{cr} (for $E–½MS_{cr}^2$) for a fixed value of S and M, respectively.

By applying this concept, the relation ($E–E_{cr}$) was multiplied with all the terms included in the corresponding existing models (Equations 2 and 3). The resulting terms were then used as predictors to regress against the respective responses using multiple regression approach. The feasibility of normalizing the relation ($E–E_{cr}$) by E_{cr} to give a dimensionless term has also been explored through the regression analysis. It was found that the normalized term has the advantage of reducing the decimal places of the coefficients of each term in the established models. Thus, the normalized relation was selected and, for simplicity, has been given a designation C ($C=(E-E_{cr})/E_{cr}$).

4.2. Maximum Residual Crush (MRC) Model

By plotting δ against M at a specific impact speed, the curves are expected to intersect the M-axis at a certain positive value that represents M_{cr}, where the initial observable crush is expected to initiate. To account for this issue and to allow the impact response of the wheel-tire assembly to include the lower region of the impact mass, which is from M=0 to 51.18 kg, an enhanced model (designated as MRC Model) has been developed to replace the initial models (Equation 2) presented in Section 2. The response δ was regressed against similar terms that have been determined to be significant and incorporated in the initial model, which are C, SC, MC, PC, SMC, SPC, SDC, MDC, and GDC. The resulting equation of the enhanced MRC model for δ is now given by:

$$\begin{aligned}\delta = C*(&-0.00811 + 0.00329*S \\ &+ 0.000267*M - 0.000044*P \\ &- 0.000047*S*M + 0.000007*S*P \\ &+ 0.00182*S*D - 0.00028*M*D \\ &+ 0.163*G*D)\end{aligned} \tag{5}$$

The value of the critical impact energy, E_{cr}, is 110.7 J, as acquired from the regression analysis in a previous work (Tan *et al*., 2006), whereby the dissipated impact energies of the wheel-tire assembly were regressed against the maximum residual crush alone.

4.3. Normalized Area of Deformation (NAD) Model

For the normalized area of deformation, the problems of not satisfying the kinetic condition also occurred for $\Delta\tilde{A}$ for the MG and MD interactions, as shown in Figures 11 and 12, respectively. To be realistic, the value of $\Delta\tilde{A}$ should be zero for both MD and MG interactions at the value of impact mass that represents M_{cr} at the specific impact speed.

An alternative improved model must be developed to resolve the problem and to predict the $\Delta\tilde{A}$ for the lower region of the impact mass, below 51.18 kg. The approach used to develop the new model discussed in Section 4.1 has also been applied here for the $\Delta\tilde{A}$. The multiple regression analysis was carried out by taking $\Delta\tilde{A}$ as the response and C, SC, MC, PC, GC, DC, SMC, MGC, MDC, and PGC as the predictors. The resulted new model for predicting $\Delta\tilde{A}$ is given by:

$$\begin{aligned}\Delta\tilde{A} = C*(&-0.000293 + 0.000505*S \\ &+ 0.000025*M - 0.00001*P \\ &- 0.0103*G + 0.00504*D \\ &+ 2.2X10^{-7}*S*M - 0.000101*M*G \\ &- 0.000042*M*D + 0.0009*P*G)\end{aligned} \tag{6}$$

The value of the critical impact energy, E_{cr}, as acquired from the simple regression analysis in a previous work (Tan *et al*., 2006), is 36.2 J, with the regression performed with dissipated energy as the response and the normalized area of deformation as predictor.

5. DISCUSSION

By plotting the initial models and corresponding newly developed models on the same graphs, their differences could be visualized much clearer. Based on the MRC Model (Equation 5), several curves have been produced by plotting the response, δ, against the impact mass, M, for several values of the offset distance of impact, D. The curves are presented in Figure 14, together with the curves from the initial model (Equation 2). Apparently, the MRC Model closely matches the initial model, especially at the low level of M (51.18 kg), where each of the curves of the new model is observed to intersect the respective curves of the initial model at an impact mass near 51.18 kg. The trend of the curves is also consistent with the previous model at both the low and the high level of M; that is, the value of δ is expected to increase as D varies from 0 to 0.108 m at the low M level and vice versa at the high M level. It can be estimated from the curves that the value of M_{cr} to produce an initial observable residual crush at the impact speed of 6 m s^{-1} (21.6 km/h) is about 6 kg. By applying the kinetic energy equation, the threshold impact energy found is $E_{cr}=(½)(6)(6)^2=108$ J. This value is very close to the value obtained from the regression analysis (Tan *et al*., 2006), which is 110.7 J.

The intersection of the curves occurs at point B, which is about 98 kg for the new model, slightly larger than that of the previous model, 85 kg (point A). However, further investigations have to be conducted for the implication of this transition value and the shift that has occurred. The data enclosed in the oval 1 correspond to the impact configuration of *sgd*, which should fall on the top curve at 51.18 kg. The data in oval 2 should match the top curve at 101.33 kg with respect to the impact configuration of *smg*. It is obvious that there is a deviation from the expected curve. However, the variation is within the acceptable range.

Three graphs have been generated based on the developed NAD Model (Equation 6), corresponding to the SM, MG, and MD interactions. Figure 15 presents one of the

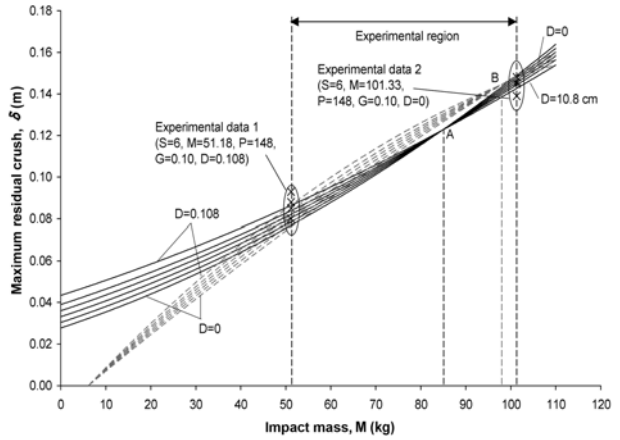

Figure 14. Curves plotted for δ versus M for the new model (Equation 5) (dashed line), compared to those for the previous model (Equation 2) in Figure 8.

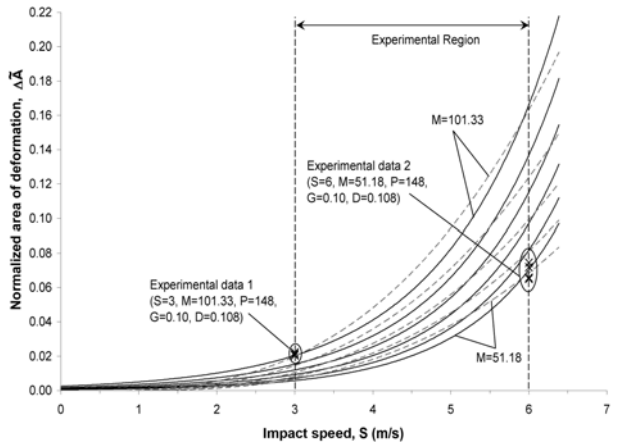

Figure 15. Curves plotted for $\Delta\tilde{A}$ versus S for the new model (Equation 6) (dashed line), compared to those for the previous model (Equation 3) in Figure 10.

graphs with several curves generated by plotting $\Delta\tilde{A}$ against impact speed for several values of impact mass at a specific P, G, and D values. The equivalent curves from the initial model (Equation 3) were plotted for comparison as well. It is obvious that the enhanced model successfully eliminated the inconsistency that existed in the initial model towards the low impact speed. Under real physical conditions, there is always a threshold value of impact speed where the impact energy is only just sufficient to yield an onset of significant deformed area on the rim. The threshold impact speed would also vary with the impact mass. These are well reflected in the curves generated from the NAD model, where the curves intersect the S-axis at different specific positive values, with lower impact mass corresponding to higher threshold impact speed. Overall, the NAD model yields higher deformed area compared to the initial model, especially for the midspan of the experimental range. Further investigation and more experimental data are required to get better insights into this observation.

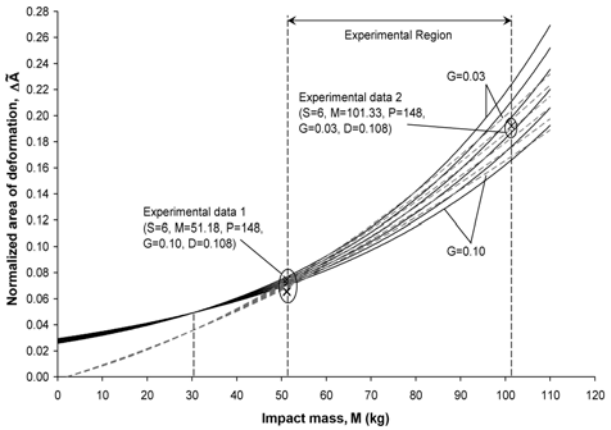

Figure 16. Curves plotted for $\Delta\tilde{A}$ versus M for the new NAD model (Equation 6) (dashed lines), compared to those for the previous model (Equation 3) in Figure 11.

However, the curve is observed to be within the range of the experimental data (cross marks on the respective lower and upper experimental regions).

For the interaction of MG, the new curves plotted are as shown in Figure 16. Overall, the model is satisfactory, as the plotted curves pass through the experimental data points at low M level, and the effect of G at low M level is relatively less significant. Also, the curves from NAD model overlap with the curves from the initial model at high M level. The trend and pattern of the curves for the enhanced model, when varying G values from 0 to 0.10 m, is also consistent to that of the initial model.

The curves that have been generated by plotting $\Delta\tilde{A}$ against M at a specific impact speed for several values of the offset distance of impact, D, are presented in Figure 17 together with the curves for the initial model. It can be seen that the NAD model closely matches the initial model within the experimental range. The curves from the initial and NAD models that correspond to a specific D value intersect each other near the impact mass of the experimental level. The trend of the curves observed for the enhanced model is also consistent with the initial model within the experimental region. At both the low and high level of M, the value of $\Delta\tilde{A}$ increases as D varies from 0 to 0.108 m at the low M level and vice versa at the high M level. It can also be observed that the curves overlapped the cross marks on the graph that represent the experimental data.

Intersections between the MG and MD curves can be seen in Figures 16 and 17, respectively. For MG interaction (Figure 16), the curves are observed to converge as impact mass is reduced and to intersect each other at point C, approximately 45 kg, higher than that for the initial model, in which they intersect at point B of about 31 kg. For MD interaction (Figure 17), the intersection of the curves from the initial model with each other occurred at point A, corresponding to about 97 kg, which is larger than that of the NAD model, estimated at about 122 kg. Further investi-

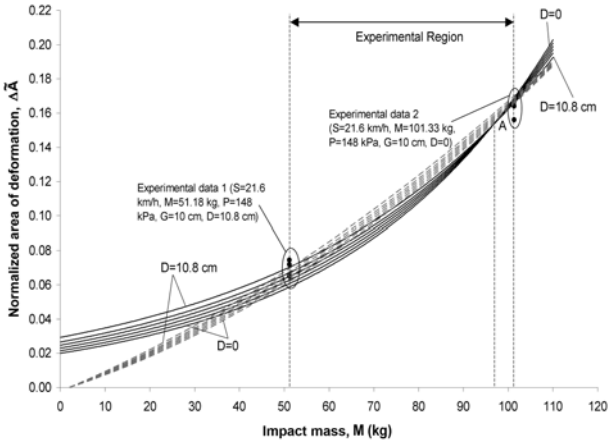

Figure 17. Curves plotted for $\Delta\tilde{A}$ versus M for the new model (Equation 6) (dashed line), compared to those for the previous model (Equation 3) in Figure 12.

gations should be conducted to determine the implication of the fact that these intersection points indicate a transition values around which the respective interactions have contrary effects on the response.

In Figure 15, the curves intersect the S-axis approximately at 1.2, 1.1, 1.0, 0.9, 0.9, and 0.8 m s^{-1}, which corresponds to the different impact masses from 51.18 kg to 101.33 kg, respectively. These impact speeds are the S_{cr} for the specific impact mass. Applying the kinetic energy equation, which is $\frac{1}{2}MS^2$, this provides the constant amount of impact energy required to yield the onset significant deformation on the rim. For example, for M=51.18 and 101.33 kg, the resulted threshold impact energy is given by $E_{cr}=(\frac{1}{2})(51.18)[(4.3)(1000/3600)]^2=36.5$ J and $E_{cr}=(\frac{1}{2})(101.33)[(3.0)(1000/3600)]^2=35.2$ J, respectively. This magnitude is very close to the value of 36.2 J which obtained from the regression analysis in a prior work (Tan *et al*., 2006). It is worth noting that the magnitude of threshold impact energy for the response $\Delta\tilde{A}$ is lower than for δ (110.7 J). This is because the general shape of the wheel was being deformed first before the localized bending that causes residual crush on the rim occurred. This implies that the rim itself is stiffer than the structural integrity of the wheel. However, this might only be true with the presence of the inflated tube and tire that provide additional cushioning to the rim.

By the same approach, from the intersection of the curves with the M-axis for both graphs in Figures 16 and 17, it is estimated that the value of M_{cr} for the impact speed of 6 m s^{-1} (21.6 km/h) is about 2 kg. Applying the kinetic energy equation, the estimated threshold impact energy is thus given by $E_{cr}=(\frac{1}{2})(2)(6)^2=36$ J, which is also very close to that from the previous work (Tan *et al*., 2006).

The experimental data for $\Delta\tilde{A}$ were plotted in the graphs shown in Figures 15, 16, and 17. The data enclosed in oval 1 in Figure 15, ovals 1 and 2 in Figure 17, and oval 2 in Figure 16, which correspond to the impact configurations of *mgd*, *sgd*, *smg*, and *smd* respectively, are expected to fall on the top curve at the corresponding limit of the experimental range. The data enclosed in oval 2 in Figure 15 and oval 1 in Figure 16 correspond to the impact configuration of *sgd* and are supposed to fall on the bottom curve at the corresponding limit of the experimental range. There are obviously some deviations of test data from the model. There is always variation between values calculated from the developed model and the experimental data. To demonstrate the variation in the MRC and NAD models, the observed experimental data of δ and $\Delta\tilde{A}$ were plotted against the predicted values obtained from the MRC and NAD models, as shown in Figures 18 and 19, respectively.

For the MRC model, the value of R^2 for the corresponding linear line is 99.71%, which is very close to that of the initial model of Equation (2), 99.94%. For the NAD model, the value of R^2 obtained is 94.84%, slightly lower than that of the initial model of Equation (3), 99.59%. It is expected that both the initial and enhanced models could be applied in predicting the deformation of wheel-tire assembly in a direct impact.

An additional regression analysis is always required in

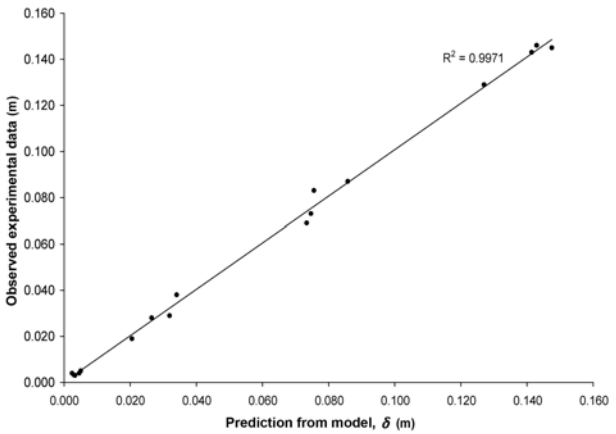

Figure 18. Observed experimental data versus predictions from MRC model for δ.

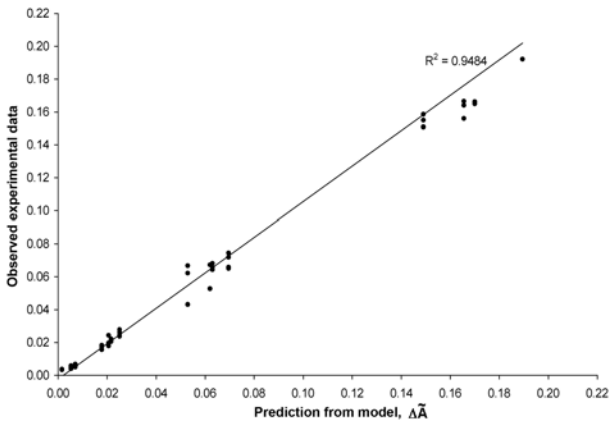

Figure 19. Observed experimental data versus predictions from NAD model for $\Delta\tilde{A}$.

further development of the new models in order to determine the critical energy of the wheel-tire assembly so that the value for C can be calculated. In general circumstances, the initial models are always adequate.

6. CONCLUSION

New models that satisfy basic physical conditions have been developed. It is anticipated that the impact response of the wheel-tire assembly, either in terms of maximum residual crush or of area of deformation, is governed by the different empirical models that correspond to the different impact mass ranges, as presented in Figures 14 and 15, respectively. For impact conditions within the experimental region, the response of the wheel-tire assembly is more reasonably predicted using the empirical models developed in earlier studies (Equations 2 and 3). However, for impact mass lower than 51.18 kg, the response can be feasibly predicted by the MRC and NAD models, given by Equation 5 for δ and Equation 6 for ΔA, respectively. However, The two new models are yet to be verified and should be applied with caution.

REFERENCES

Fujii, S. (2003). Motorcycle tire crash analysis. *Yamaha Motor Technical Review*, Dynamics Department Advanced Technology Research Division, Yamaha Motor, Japan.

Harms, P. L. (1989). Leg injuries and mechanisms in motorcycle accidents. *Proc. 12th Int. Conf. Experimental Safety Vehicles*. Gothenburg, Sweden.

Hight, P. V., Nevhall, P. E. Langwieder, K. and Mackay, G. M. (1986). An international review of motorcycle crashworthiness. *Int. IRCOBI Conf. Biomechanics of Impacts.* Zurich, Switzerland, 261–276.

Minitab (2000). *User's Guide 2: Data Analysis and Quality Tools*. Version 13. Minitab Inc. Pennsylvania. USA.

Montgomery, D. C. (2001). *Design and Analysis of Experiments*. 5th edn. John Wiley & Sons. New York. USA.

Otte, D., Kalbe, P. and Surgen, E. G. (1981). Typical injurie to the soft body parts and fractures of the motorised 2-wheelers. *Proc. 6th IRCOBI Conf. Biomechanics of Impacts*, Salon de Provence, France, 148–165.

Pang, T. Y., Radin Umar, R. S., Azhar, A. A., Harwant, S., Shahrom, A. W., Abdul Halim b. Hj, M., Zahari, N. and Mohd Shafie bin Othman (1999). Fatal injuries in Malaysian motorcyclists. *Int. Medical Research J.* **3**, **2**, 115–119.

Sporner, A., Polauke, J. and Driessche, H. V. (1995). Collision parameters from real-life car/motorcycle zccidents-A basis for future standards. *SAE Paper No*. 950203. 381–388.

Tan, K. S., Wong, S. V., Hamouda, A. M. S., Megat Ahmad, M. M. H. and Radin Umar, R. S. (2004). *MechT™ Impactor-Engineering Design and Specifications*. Universiti Putra Malaysia.

Tan, K. S., Wong, S. V., Radin Umar, R. S., Hamouda, A. M. S. and Gupta, N. K. (2006). An experimental study of deformation behaviour of motorcycle front wheel-tyre assembly under frontal impact loading. *Int. J. Impact Engineering*, Elsevier **32**, **10**, 1554–1572.

Whitaker, J. (1980). *Survey of Motorcycle Accidents*. TRRL Laboratory Report LR913. Transport and Road Research Laboratory. Crowthorne. Berkshire. U.K.

Yettram, A. L., Happian-Smith, J., Mo, L. S. M., Macaulay, M. A. and Chin, B. P. (1994). Computer simulation of motorcycle crash tests. *14th Int. Conf. Enhanced Safety of Vehicles*. Munich, Germany, 23–26.